The Crustal and Upper Mantle Velocity Structure of the Southern Korean Peninsula from Receiver Functions and Surface-Wave Dispersion

H. J. Yoo[1), 2)], K. Lee[1)], R. B. Herrmann[3)]

[1)]School of Earth and Environmental Science, Seoul National University.
[2)] Korea Polar Research Institute, KORDI.
[3)] Department of Earth and Atmospheric Sciences, Saint Louis University.

수신함수와 표면파 분산의 동시역산을 이용한 한반도 남부지역의 지각과 상부맨틀 연구

유현재[1), 2)], 이기화[1)], R. B. Herrmann [3)]

[1)]서울대학교 지구환경과학부, hjyoo5@snu.ac.kr
[2)] 해양연구원 부설 극지연구소.
[3)] Department of Earth and Atmospheric Sciences, Saint Louis University.

Abstract : 3-D S-wave velocity model in the southern Korean Peninsula is investigated by using the joint inversion of receiver functions and surface-wave dispersion. A peninsula average Rayleigh-wave phase velocity in the 10-150 seconds range and tomographic estimates of the Rayleigh and Love wave group velocities in the 0.5-20 seconds period range determined using a 12.5 x 12.5 km grid for the southern part of the peninsula are used for the inversion. Receiver functions were determined from broadband (STS-2), short-period (SS-1) and acceleration (Episensor) channels of 95 stations. The dense distribution of the stations in the Peninsula permits us to examine the 3-D crustal structure in detail. The inversion result shows the variation and characteristics of S-wave velocity in the crust and upper mantle of the southern Korean Peninsula very well.
Keywords : joint inversion, receiver function, surface-wave dispersion, 3-D crustal structure

요약 : 이 연구에서는 수신함수와 표면파 분산을 동시역산하는 방법을 통해 한반도 남부지역의 3-D S-파 속도모델을 구하였다. 10-150 초 주기의 한반도 평균 레일리 위상속도 데이터와 12.5 x 12.5 격자의 레일리파 및 러브파 토모그래피 결과로부터 얻은 0.5-20 초 주기의 군속도 자료가 역산에 사용되었다. 수신함수는 95 개 관측소의 광대역(STS-2), 단주기(SS-1), 및 가속도(Episensor) 채널로부터 계산되었다. 한반도에 운영중인 조밀한 지진관

측소 분포는 3-D 지각구조의 자세한 연구를 가능하게 한다. 역산 결과 한반도 남부 지역의 지각과 상부맨틀의 S-파 속도변화와 특성을 자세히 관찰할 수 있었다.

주요어 : 동시역산, 수신함수, 표면파 분산, 3-D 지각구조

1. Introduction

In virtue of the advent of digital seismometry and improvements in station coverage from late 1990s, the receiver function method (Kim and Lee, 2001; Yoo and Lee, 2001; Chang and Baag, 2005) has been applied to study the crust and upper mantle structure in and around the Peninsula, providing more reliable information on the seismic velocity changes of the crust in detail. However, due to the small number of broadband stations used and methodology itself, they could not image the Peninsula in a manner to address the fundamental questions, crustal evolution.

Here we used the receiver function data, sensitive to velocity transitions and vertical travel times, together with surface-wave dispersion measurements, sensitive to average of the velocities and relatively insensitive to sharp velocity contrasts, to estimate the variations of crustal structure and the character of Moho discontinuity of whole southern part of the Korean Peninsula. This approach minimizes the trade-off between crustal thickness and wave speeds when receiver function or dispersion of surface waves is analyzed separately (Özalaybey et al., 1997; Julia et al., 2000). Our effort differs from previous studies in three important ways. First, we use receiver functions at 59 sites on the southern Korean peninsula. Second we use Korean seismic data to determine a dense distribution of Rayleigh wave phase velocities in the 10-150 second period range. Finally, we use the results of surface-wave group velocity tomography tomography in the 1-20 second period range (Cho et al., 2006).

2. Digital seismic data

Digital seismology in Korea began with the installation of the IRIS station that is now at Inchon. Subsequently the Korean Institute of Geoscience and Mineral Resources (KIGAM) installed some broadband stations. In 2000, the Korean Meteorological Administration (KMA) digital seismic network became operational. The KMA network has a backbone of broadband stations, some additional short-period stations, and a dense network of accelerometers transmitting continuous data to the analysis center in Seoul. In addition additional broadband sensors are operated by Korea Institute of Nuclear Safety (KINS). Although we didn't use the data in this study, additional broadband sensors and accelerometers are operated by the Korean Electric Power Research Institute (KEPRI). For the surface-wave

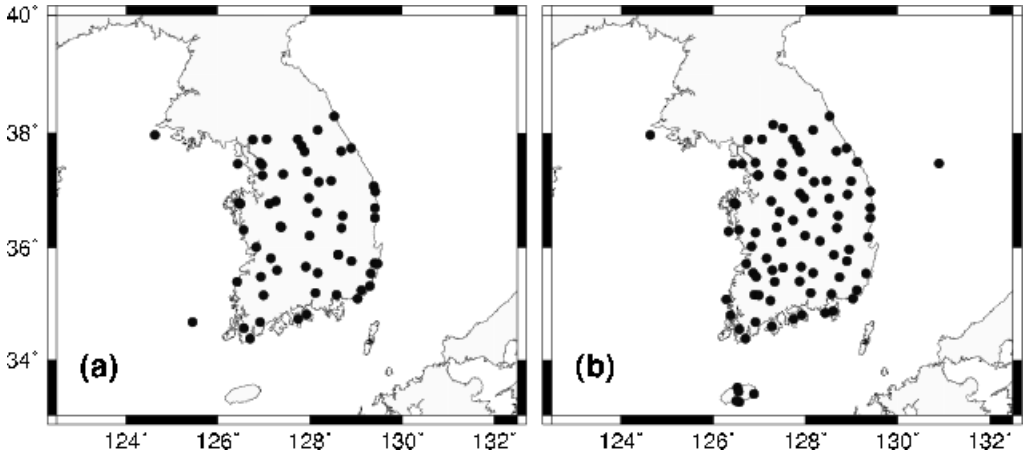

Figure.1. Location of stations used in this study. (a) stations use for receiver function determination. (b) stations used for group velocity determination from inter-station Green;s functions from the cross-correlation of ground noise.

studies we used data from the broadband stations of KMA and KIGAM, approximately 15 at the time, for phase velocity determination, and waveforms from KMA broadband and acceleration channels for the group velocity analysis (Cho. et al., 2006). Receiver functions were determined from the KMA, KIGAM and KINS broadband channels and selected KMA short-period and acceleration channels. Figure 1 presents the location of the sites providing the group velocities and the receiver functions that we used in the study. The dense distribution of the stations permits us to examine the 3-D crustal structure in detail.

3. Surface-wave dispersion

The surface-wave data consists of two components, which are a peninsula average Rayleigh-wave phase velocity in the 10-150 seconds range and tomographic estimates of the Rayleigh and Love wave group velocities in the 0.5-20 seconds period range determined using a 12.5 x 12.5 km grid for the southern part of the peninsula.

To obtain the phase velocities at longer periods, we applied the p-omega technique of McMechan and Yedlin (1981) to teleseismic Rayleigh waves observed on the Peninsula. The fundamental mode surface-wave was extracted using a combination of multiple filter analysis and phase matched filtering, a great circle path was assumed to project the station observations onto a pseudo-linear array for analysis, and the phase velocities were determined. The Korea average Rayleigh wave phase velocity dispersion was determined in the 10-150 period range from about ten distant earthquakes. In spite of scatter, at the longer periods, the dispersion agreed with the Harvard tomography.

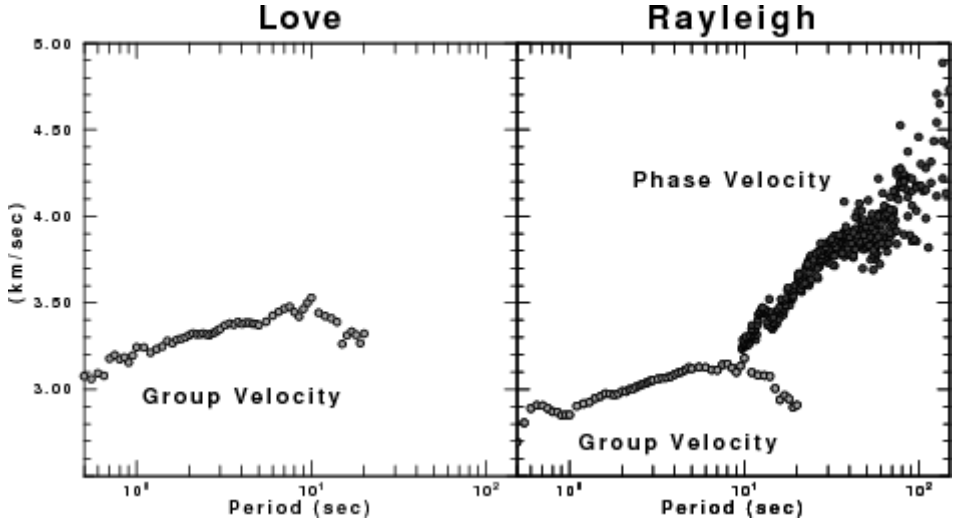

Figure. 2. Dispersion used for the station CHJ (36.87N, 127.97E). The group velocities are indicated by the lighter shade of gray, and the phase velocities by the darker.

Cho et al (2006) derived tomographic maps of Rayleigh- and Love-wave group velocity dispersion from inter-station empirical Green's functions obtained from the cross-correlation of ground noise (Shapiro et al, 2005). Group velocities obtained from the empirical Green's functions for over 2100 inter-station paths in the 0.5-20 second period band. Because of the path density, they used a 12.5 x 12.5 km grid to create a tomographic dispersion image for each measured period. For our application, we associate the dispersion at a station with the nearest tomographic grid value. This is justified by the wavelengths considered and the smoothing used for the tomography. Figure 2 shows the dispersion data used at the KMA station CHJ.

4. Receiver functions

Receiver functions are filters which predict a filtered version of a horizontal component from the vertical component trace (Ammon, 1997). This study uses P-wave radial receiver functions. To obtain these, teleseismic waveforms with a good P-signal are selected. The receiver function is estimated using the iterative time-domain deconvolution technique of Ligorria and Ammon (1999), which is an implementation of the Kikuchi and Kanamori (1982) technique. The time-domain Gaussian pulses used correspond to low-pass filters with frequencies of 0.3 and 1.0 Hz. Because of signal-to-noise, we found it difficult to work with any processing that focused on higher frequencies. In addition we did not try to use longer time-domain pulses, e.g., lower frequency data, because of long-period noise and because of the limited resolution of such data. In the terminology of Ligorria and Ammon (1999), we used the filter parameters alpha = 1.0 and 2.5.

A multi-step process was used to determine if a given receiver function should be used in the inversion for structure. The first criteria required that the derived receiver function predict 80% of the filtered radial signal power. This criteria is a quality check on the deconvolution stage. Unrealistic receiver functions with the first negative pulse, passed this criteria since the deconvolution is a purely mathematical procedure that knows nothing of elastic wave propagation. Given large data sets, we excluded these data manually.

The second criteria involved using all acceptable receiver functions for the joint inversion of surface-wave dispersion and receiver function at a station. The reduction of variance between each observed and predicted receiver function is obtained from this process. Predictions are made for the final crustal model and are thus constrained by elastic wave propagation theory. Of all the receiver functions used, we used only those that fit 80% of the observed signal power. This stage rejected many signals for the final inversion. Of the 95 stations initially considered, only 56 stations have 6 or more good receiver functions. The locations of these stations are shown in Figure 1a.

We were able to have so many stations available for analysis because we obtained receiver functions from broadband (STS-2), short-period (SS-1) and acceleration (Episensor) channels of the 20Hz archived data stream. Since STS-2 and SS-1 sites also had episensor channels, we were able to verify that the acceleration channels could give good receiver functions. The possibility of using the acceleration channels was suggested by the success in obtaining empirical inter-station Green's functions from them, which is because these channels in Korea are more sensitive than is typical.

The use of these data is made easier since there seems to be little azimuthal dependence on the receiver function and since the P-wave transverse receiver function is usually small.

5. Joint inversion procedure and results

Joint inversion of receiver functions and surface-wave dispersion was first proposed by Özalaybey et al (1997). It has been used by Juliá et al (2000), Herrmann et al (2001) and Chang and Baag (2005). The iterative least-squares joint inversion used here is described by Herrmann and Ammon (2002). Surface-wave dispersion partial derivatives are computed analytically while receiver function partial derivatives are computed numerically. The inversion fixes the Vp/Vs ratio in each layer and recomputes layer density from the P-wave velocity after each iterations. A differential smoothing constraint is applied with the objective of finding the simplest model that fits the data set. The smoothing constraint is

implemented by solving for the change in the velocity contrast at layer boundaries rather than solving for the changes in the individual layer velocities. The starting model used at all sites consists of 85 layers to a depth of 580 km. From a depth of 50 km to the bottom, the model is AK135-F Continental Model (http://wwwrses.anu.edu.au/seismology/ak135/ak135f.html). The upper 50 km of the model consists of layers (four 1 km and twenty-three 2 km) having the same velocities as AK135-F at 50 km. The velocity jumps at the layers boundaries are not permitted to change from 380 km to the bottom of the model. They are permitted to change slightly from 80-380 km, and to change more freely in the upper 80 km. The high initial velocities of the crust provide a uniform unbiased starting model for the inversion. No a-priori assumptions about the location of the Moho are made. In addition no persistent artifacts of crustal layer boundaries appear in the solution. Starting with a continental upper mantle, and permitting a significant departure from the starting model only in the upper 80 km, ensures that the lower part of the model does not depart from the global seismology experience. The choice of crustal layer thicknesses of 2.0 km is appropriate because of the lack of resolution with fundamental mode surface-wave dispersion, and the receiver function resolution for the filters used.

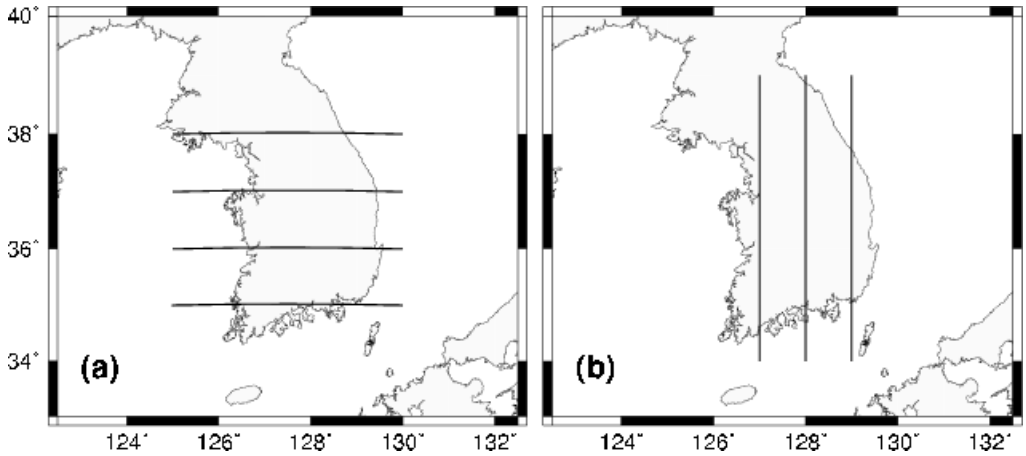

Figure. 3. Center lines for the depth sections shown in Figures 5 for (a) and 6 for (b).

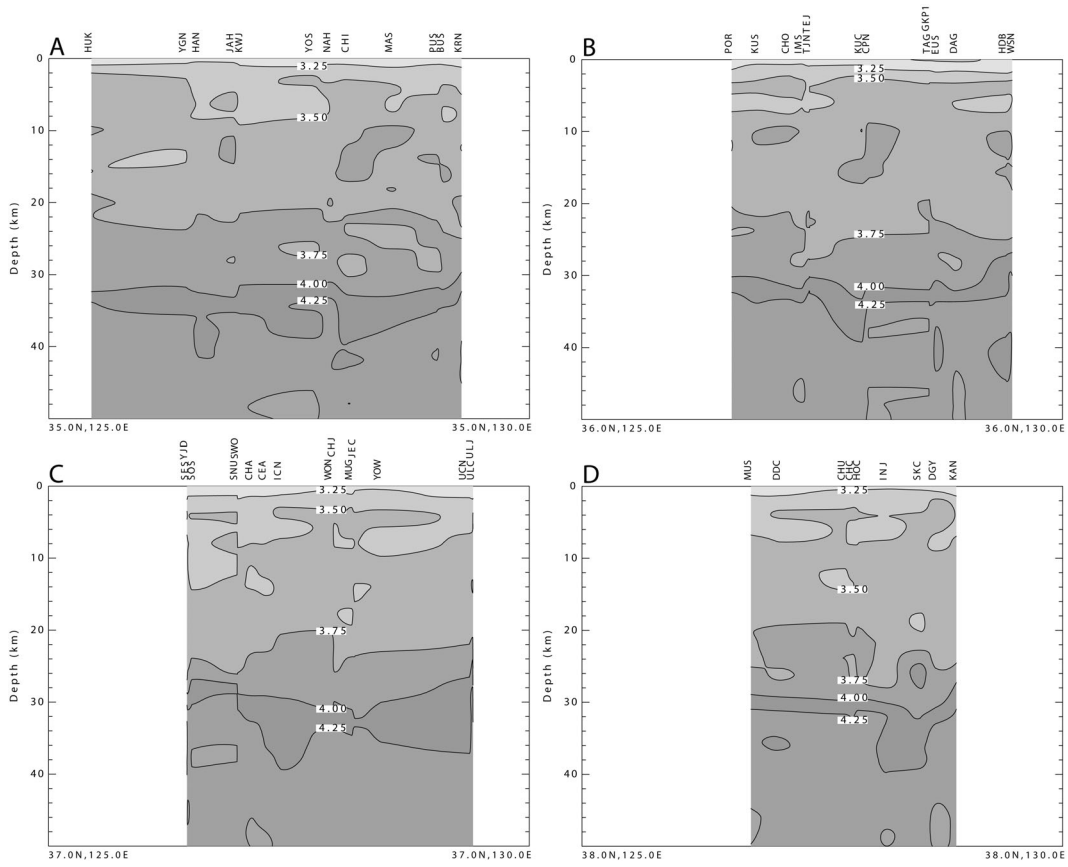

Figure. 4. East-west S-wave velocity profiles from south(A) to north(D). Figure 3a shows the profiles. The coordinates of the profile are given at the bottom of each plot. Contours are given at every 0.25 km/sec and the 3.5 and 4.0 km/sec contours are indicated.

As mentioned above, we performed the joint inversion twice, first with all receiver functions associated with a successful deconvolution, and second with just those for which the model provided at least an 80% variance reduction in fit. Since it is the receiver functions which provide the constraints on velocity model discontinuities, we will focus only on those 56 sites which had 6 or more receiver functions. At common stations, we have compared our inverted models with those from the recent work of Chang and Baag (2005). The models are quite similar.

Rather than presenting all 56 models, and to test the usefulness of our approach to image the three-dimensional crust, we present the results as vertical sections. These are shown in Figure 3. The S-wave velocity models of all stations 50 km on either side of each will contribute to the plot. The perpendicular from the station to the profile is used to project the station model along the profile. The FORTRAN contouring program FARB2D by Preusser (1986) is used. Contours were made at intervals of 0.25 km/s with the 3.5 and 4.25 km/s contours labeled. Except for a few places near the surface, all of the S-wave velocities are greater

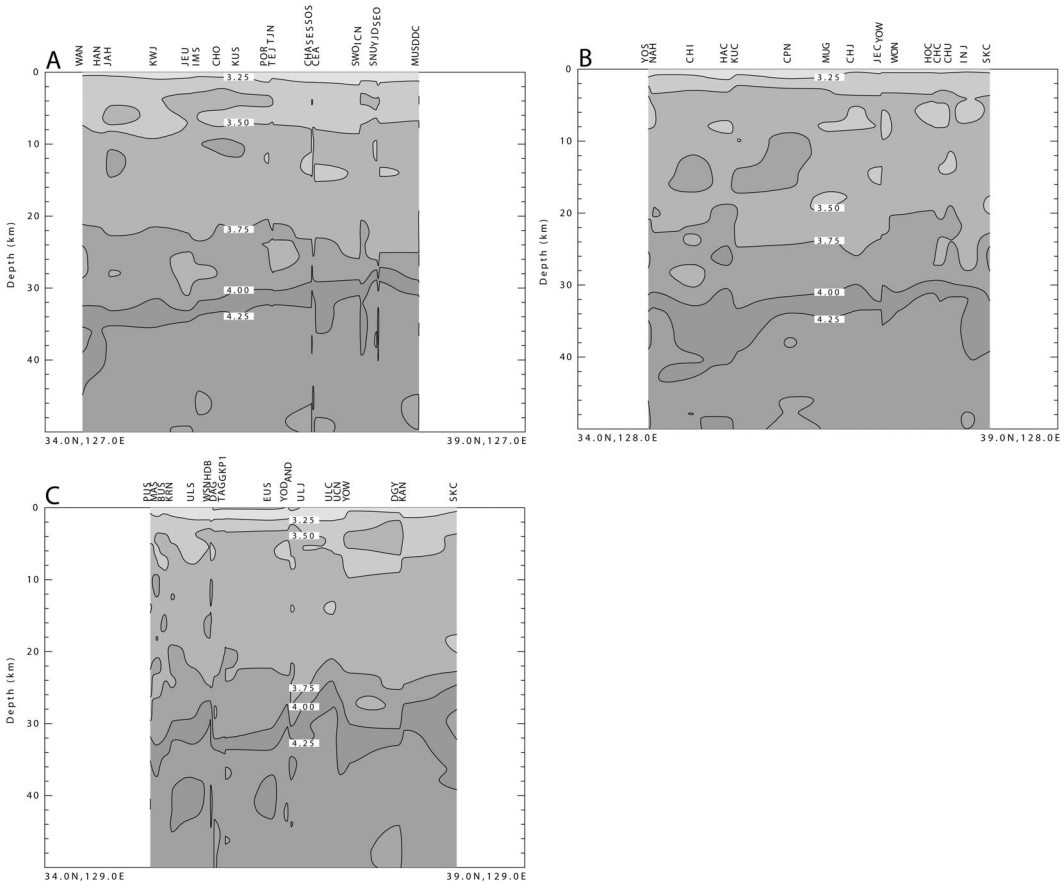

Figure 5. South north S−wave profiles from west to east. . Figure 3b shows the profiles. The coordinates of the profile are given at the bottom of each plot. Contours are given at every 0.25 km/sec and the 3.5 and 4.0 km/sec contours are indicated.

than 3.0 km/s. Almost all models have a slightly lower velocity upper crust overlying a relatively uniform velocity mid−crust. We can find that the sharp velocity discontinuity between crustal and upper mantle velocities generally had a mid−velocity of 4.2 km/sec, which we take as proxy for the location of the Moho.

These images are complicated and show the artifacts of the contour routine used as well as the inconsistencies of some of the inversions. Focusing on the west−east profile at 37N (Figure 4C), we see some vertical contours on the figure to the left of station CHA. This is because the models at SWO and SNU do not agree. There are extreme examples of individual disagreement in Figure 5A.

The crustal thickness varies from about 26 km to about 36 km. The deepest Moho i s found beneath the ridge in southwestern part of the Peninsula (See Figure 4A). S mallest values that are found in off−shore region to East Sea are likely affected by t ransitional procedure to oceanic crust. Moho is deeper as it goes from north to sout h and central part of the Peninsula. The general trend of the depth distribution of M oho (has about shear velocity of 4.2 km/s) is similar to that of previous results (Cho et al., 2006; Chang and Baag, 2005).

References

Ammon (1997). An overview of receiver-function analysis, http://eqseis.geosc.psu.edu/~cam-mon/HTML/RftnDocs/rftn01.html.

Chang, S. and C. Baag (2005). Crustal Structure in Southern Korea from Joint Analysis of Teleseismic Receiver Functions and Surface-Wave Dispersion, Bull. Seism. Soc. Am., 95, 1516-1534.

Cho, H., C. Baag, J. M. Lee, W. M. Moon, and H. Jung (2006). Crustal velocity structure across the southern Korean Peninsula from seismic refraction survey, Geophy. Res. Lett., 33, 1-4.

Cho,. K.H., R. B. Herrmann, C. J. Ammon, and K. Lee (2006). Imaging the crust of the Korean Peninsula by surface-wave tomography , Bull. Seism. Soc. Am., in review.

Herrmann, R. B., C. J. Ammon, and J. Juliá (2001). Application of joint receiver-fucntion surface-wave dispersion for local structure in Eurasia, 23rd Seismic Research Review: Worldwide Monitoring of Nuclear Explosions - October 2-5, 46-54.

Herrmann, R. B., and C. J. Ammon (2002). Computer Programs in Seismology 3.30: Surface waves, receiver functions and crustal structure, http://www.eas.slu.edu/People/RBHerrmann/CPS330.html.

Juliá, J., C. J. Ammon, R. B. Herrmann, and A. M. Correig (2000). Joint inversion of receiver function and surface wave dispersion observations, Geophys. J. Int. 143, 99-112.

Kikuchi, M. and H. Kanamori (1982). Inversion of complex body waves, Bull. Seism. Soc. Am. 72, 491-506.

Kim, S. G. and S. K. Lee (2001). Moho discontinuity studies beneath the broadband stations using receiver functions in South Korea, Korean Soc. Hazard Mitigation 1, 139-155.

Ligorria, J. P. and C. J. Ammon (1999). Iterative deconvolution of teleseismic seismograms and receiver function estimation, Bull. Seism. Soc. Am. 89, 1395-1400.

McMechan, G. A. and M. J. Yedlin (1981). Analysis of dispersive waves by wave field transformation, *Geophysics* 46,869-874.

Özalaybey, S., M. K. Savage, A. F. Sheehan, J. N. Louie, and J. N. Brune (1997). Shear-wave velocity structure in the northern Basin and Range province from the combined analysis of receiver functions and surface waves, Bull. Seism. Soc. Am. 87, 183-199.

Preusser, A (1986). Computing area filling contours for surfaces defined by piecewise polynomials, Computer Aided Geometric Design 3, 267-279.

Shapiro, N.M. M. Campillo, L. Stehly, and M.H. Ritzwoller (2005). High resolution surface wave tomography from ambient seismic noise, Science, 307(5715), 1615-1618.

Yoo, H. and K. Lee (2001). Crustal structure under the Taejon(TJN) station by receiver function methods, J. Korean Geophy. Soc. 4, 35-46.